1994ApJ...437..879A

THE ASTROPHYSICAL JOURNAL, 437:879–891, 1994 December 20
© 1994. The American Astronomical Society. All rights reserved. Printed in U.S.A.

LOW-TEMPERATURE ROSSELAND OPACITIES

D. R. ALEXANDER AND J. W. FERGUSON[1]
Physics Department, Wichita State University, Wichita, KS 67260
Received 1994 March 21; accepted 1994 June 22

ABSTRACT

A new, comprehensive set of low-temperature opacity data has been assembled. From this basic data set, Rosseland and Planck mean opacities have been computed for temperatures between 12,500 and 700 K. In addition to the usual continuous absorbers, atomic line absorption (with more than 8 million lines), molecular line absorption (with nearly 60 million lines), and grain absorption and scattering (by silicates, iron, carbon, and SiC) have been accounted for. The absorption due to lines is computed monochromatically and included in the mean with the opacity sampling technique. Grains are assumed to form in chemical equilibrium with the gas and to form into a continuous distribution of ellipsoids.

Agreement of these opacities with other recent tabulations of opacities for temperatures above 5000 K is excellent. It is shown that opacities which neglect molecules become unreliable for temperatures below 5000 K. Triatomic molecules become important absorbers at 3200 K. Similarly, grains must be included in the computation for temperatures below 1700 K.

Subject headings: atomic — molecular data

1. INTRODUCTION

Whenever energy is transported by radiative processes a knowledge of the opacity of the medium is required in order to compute the thermal structure of the material. In those cases where the diffusion approximation is applied to the transfer of energy, the Rosseland mean opacity, defined as

$$\frac{1}{\kappa_R} = \int_0^\infty \frac{1}{\kappa_\nu}\frac{\partial B_\nu}{\partial T}\,d\nu \Big/ \int_0^\infty \frac{\partial B_\nu}{\partial T}\,d\nu\,, \qquad (1)$$

is required. Because this average is an inverse average of the monochromatic opacity, it can be strongly affected by wavelengths near the peak of the weighting function which have relatively little opacity. If bound-bound absorption by atoms or molecules is significant, this factor requires that the most complete line lists possible, including very many weak lines whose combined effect may veil some frequencies even though the lines individually would be negligible, must be assembled in order to produce accurate Rosseland means.

For more than 30 years investigators at Los Alamos National Laboratory have provided Rosseland mean opacities for use in stellar modeling (see, for example, Cox & Stewart 1965; Cox & Tabor 1976; and Weiss, Keady, & Magee 1990). Several groups have recently reexamined the task of computing frequency-averaged opacities (Rogers & Iglesias 1992 [OPAL]; Seaton et al. 1994 [OP] and references therein), and in the process they have made significant progress toward explaining several discrepancies between models and observations of pulsating stars (Iglesias, Rogers, & Wilson 1990). However, all of these projects focused their attention on the conditions found in stellar interiors and stellar envelopes.

With the exception of Weiss et al. (1990), who included unspecified molecular absorbers and considered temperatures as low as 1500 K, none of these groups has considered opacities for the conditions which occur in the outer layers of cool giant stars or in star-forming clouds. The computation of opacities at temperatures below about 5000 K is complicated by the formation of molecules and the myriad spectral lines they possess. When temperatures below about 1700 K are encountered, grain equilibrium and the complex absorption processes of grains must also be included. It is this range of conditions which forms the focus of this paper.

Early compilations of low-temperature opacities by Cameron & Pines (1973) and Alexander (1975) included simple equilibrium calculations for grains and crude approximations for the opacities of both molecules and grains. Alexander, Johnson, & Rypma (1983, hereafter AJR) compiled more extensive results which included detailed treatment of grain equilibrium, consideration of a wider range of solid and molecular absorbers, and the effects of the grain size distribution. Sharp (1992) published tables of Rosseland and Planck mean opacities which included a detailed consideration of the line spectra of many diatomic and two triatomic (H_2O and CO_2) molecules. Pollack, McKay, & Christofferson (1985) and Pollack et al. (1994) also completed extensive calculations of Rosseland opacities, but only for conditions in which solid particles condense.

For this investigation Rosseland and Planck mean opacities have been computed over the range of temperature from 700 to 12,500 K and density from $\log R = -7.0$ to $+1.0$, where $R = \rho/T_6^3$, ρ is the density in g cm^{-3}, and T_6 is the temperature in millions of degrees (see OPAL for discussion). Tables can be constructed with either R or ρ as an independent variable. Tables utilizing R have the advantage that the relevant parameter range can be covered with a rectangular table and it has also been shown (OPAL) that interpolation in tables of R is more accurate. Unless specified otherwise, all opacities will be presented in mass units (cm^2 g^{-1}) in this paper.

All opacities are computed with the opacity sampling (OS) technique with a set of 9279 frequencies in the range 0.10–100 μm. Numerical tests indicate that the rms error introduced by the use of this truncated frequency set (compared to an infinitely large set of frequencies) is less than 3% for the worst case, and usually much less. Such errors are acceptable compared to the uncertainties in the monochromatic opacities themselves.

[1] Now at Department of Physics & Astronomy, University of Kentucky, Lexington, KY 40506.

© American Astronomical Society • Provided by the NASA Astrophysics Data System

1994ApJ...437..879A

2. EQUATION OF STATE

In this study it has been assumed that the medium is in local thermodynamic equilibrium and that all species are in strict chemical equilibrium. This assumption permits the equation of state (EOS) to be written in terms of the appropriate equilibrium equations for each species. These equations are solved using the subroutines described in Kurucz (1970, hereafter K70), which were modified to include grain condensation, as described in AJR. Briefly, the percentage of each element which is condensed is tabulated as a function of temperature and pressure from a detailed consideration of the condensation equilibrium. Each time the EOS subroutines are called from within an opacity calculation, the abundance of each condensable element remaining in the gas phase is reduced from its original abundance by the percentage of that element which is condensed at the given temperature and pressure. We have used condensed percentages for C, O, Si, Mg, Fe, Ti, and Zr for a variety of compositions with differing C/O ratios provided by Sharp (1989) which are based upon the detailed condensation equilibrium calculations described in Sharp & Huebner (1990).

The EOS includes a wide variety of atomic and molecular species because of the wide range of temperatures and densities included in the opacity tables. Table 1 lists the atomic species included in the EOS. All atomic partition functions have been taken from K70. Several of the heavier elements are included because they form molecules which are opacity sources or are important for spectroscopic analyses of late-type stars.

Table 2 lists the molecular species included in the EOS, along with the source of the partition function for each species.

TABLE 1

ATOMIC SPECIES INCLUDED IN EOS

Species	States Included
H	I, II
He	I, II
C	I, II, III
N	I, II, III
O	I, II, III
F	I
Ne	I, II
Na	I, II, III
Ng	I, II, III
Al	I, II, III
Si	I, II, III
P	I, II, III
S	I, II, III
Cl	I, II, III
Ar	I, II
K	I, II, III
Ca	I, II, III
Sc	I, II, III
Ti	I, II, III
V	I, II, III
Cr	I, II, III
Mn	I, II, III
Fe	I, II, III
Co	I, II, III
Ni	I, II, III
Cu	I, II, III
Zn	I, II, III
Sr	I, II
Y	I, II
Zr	I, II
Tc	I, II
Ba	I, II
La	I, II

TABLE 2

MOLECULAR SPECIES INCLUDED IN EOS

Molecule	Source of Partition Function
H_2	I87
H_2^+	ST
HF	ST
HCl	ST
CH	ST
C_2	ST
CN	ST
CO	I87
CS	ST
NH	ST
N_2	ST
NO	ST
NS	ST
OH	ST
O_2	ST
NaH	ST
MgH	ST
MgO	ST
AlH	ST
AlO	ST
AlF	ST
AlCl	ST
SiH	ST
SiO	ST
SiS	ST
SH	ST
SO	ST
S_2	ST
CaH	ST
TiO	ST
TiO^+	GG
VO	ST
YO	ST
ZrO	ST
ZrO^+	GG
H_3^+	SMT + CGP
H_2O	I88
HCN	I88
HCO	I88
CH_2	I88
C_2H	I88
C_3	I88
CO_2	I88
AlOH	I88
SiC_2	I88
TiO_2	I88
VO_2	I88
ZrO_2	I88
CH_3	I88
C_2H_2	I88
CH_4	I88

REFERENCES.—ST = Sauval & Tatum 1984; I88 = Irwin 1988; SMT = Sidhu, Miller, & Tennyson 1992; I87 = Irwin 1987; GG = Gurvich & Glushko 1982; CGP = Chandra, Gaur, & Pande 1991.

Again the list is diverse in order to accommodate a wide range of chemical compositions. The selection of species was guided by the calculations of Johnson & Sauval (1982) and Irwin (1988). Several polyatomic species containing heavy elements are included because they may affect the abundance of an opacity source.

Two special notes should be made about the molecular equilibrium calculations. First, TiO^+ and ZrO^+ are included because they can significantly affect the equilibrium abundance of the important opacity sources TiO and ZrO in a narrow

© American Astronomical Society • Provided by the NASA Astrophysics Data System

1994ApJ...437..879A

range of temperatures and densities. For example, at 2500 K and a density of 10^{-10} g cm^{-3}, the abundance of ZrO is depressed by a factor of 4 when ZrO^+ is included in the calculation. The effect of TiO^+ is much smaller, reaching a maximum of about 1% at 2500 K.

Secondly, Lenzuni, Chernoff, & Salpeter (1991) have pointed out that H_3^+ can significantly affect the abundance of H^- in metal-free gases by contributing additional free electrons. We have taken its partition function from Sidhu, Miller, & Tennyson (1992) for temperatures below 2500 K and equal to 1.793 times the values given by Chandra, Gaur, & Pande (1991) at higher temperatures. The scaling factor is required to smoothly match the values at 2500 K. The Chandra et al. (1991) values are significantly lower than those given by Sidhu et al. (1992), apparently because they did not include as many energy levels in their analysis. Further work is needed to resolve this uncertainty. Fortunately, the influence of H_3^+ is negligible whenever metals (elements heavier than He) have a mass fraction greater than or equal to 0.0001.

3. OPACITY SOURCES

The opacity sources described here allow for the accurate tabulation of Rosseland and Planck mean opacities for temperatures between about 700 and 12,500 K. Because this temperature range includes a wide variety of different types of absorption and scattering processes from many diverse species of atoms, molecules, and dust grains, the number and variety of opacity sources which must be included is extensive. Even though many of them are computed with rather standard methods or subroutines, an attempt will be made to describe all of the opacity sources so that complete references will be available in one location.

3.1. *Atomic Absorption*

3.1.1. *Continuous Sources*

The bound-free and free-free absorption of H I and He I is computed as described in K70. The bound-free absorption of H^- is computed from the fitting formula of John (1988) to the cross-sections of Wishart (1979). The free-free absorption of H^- is computed from the fitting formula of John (1988) to the cross sections of Bell & Berrington (1987).

The bound-free absorption of the following species is included using the formulation of K70 (number of levels in parenthesis): N I (3), O I (1), Mg II (2), Si II (5), and Ca II (3). In addition, the bound-free absorption of C I (8), Mg I (8), Al I (8), Si I (8), and Fe I (15) are computed using subroutines originally derived from the Pandora NLTE program (Vernazza, Avrett, & Loeser 1980). Bound-free absorption of Na I (8) and Ca I (8) are similarly derived from Pandora (Avrett 1987).

3.1.2. *Spectral Line Sources*

Atomic line data for the neutral and first ionization stage of the elements Ca–Ni is taken from Kurucz (1991). Data for a few other elements is taken from Kurucz & Peytreman (1975). Table 3 lists the elements and the number of lines included for each ionization stage. Only the strongest lines of doubly ionized elements are included because those species are not important at the temperatures of interest here.

For each line the strength factor

$$S = gf \frac{AB_i}{AB_{\rm Fe}} e^{-E_l/kT} \qquad (2)$$

TABLE 3

THE NUMBER OF SPECTRAL LINES INCLUDED FOR EACH ELEMENT

Element	Species I	Species II	Species III
C	1679	152	9
N	2616	686	
O	416	909	32
F	854	594	
Ne	1109	2646	
Na	152	22	11
Mg	638	233	40
Al	98	1501	14
Si	1926	221	66
P	724	404	3
S	277	383	6
Cl	1491	718	15
Ar	1371	2913	
Ca	25585	890	7
Sc	191264	49568	59
Ti	867399	248075	2
V	853786	808584	1
Cr	338668	1007782	50
Mn	248165	575578	19
Fe	579105	921100	148
Co	372937	714857	291
Ni	102224	284434	20
Cu	181	2041	14

is defined, where AB_i is the fractional number abundance of the element, $AB_{\rm Fe}$ is the fractional number abundance of iron, and E_l is the energy of the lower level of the transition. Lines are then divided into three categories according to the strength factor for the line. All lines with $S < 10^{-5}$ are weak lines. They are included in the calculation only if they fall within 4 Doppler half-widths of a sampling frequency. Since sampling frequencies are never that close together, these lines contribute to the opacity at only one sampling frequency.

Lines with $S \geq 0.025$ are strong lines. The absorption coefficient of each strong line is computed with a Voigt profile, with the damping constant equal to 3 times the classical radiation damping constant plus the van der Waals collisional damping constant (Unsöld 1955). The microturbulent velocity is set to 2.0 km s^{-1} from studies of red giant stars (Smith and Lambert 1985, 1986, 1990). Strong lines are tested at each wavelength, but are included in the opacity only if

$$N_i \alpha_0 \frac{\Gamma}{x^2} \geq 10 , \qquad (3)$$

where N_i is the number density of the absorbing species, α_0 is the absorption at line center, Γ is the damping constant for the line, and $x = \Delta\nu/\Delta\nu_{\rm D}$ measures the number of Doppler half-widths between the sampled frequency and line center. The maximum error introduced by the use of this approximation at any temperature-density point is less than 0.5%. Its use speeds up the computation significantly because far fewer evaluations of the Voigt function are required. Following OP, the wings of the strong lines are reduced in strength by the factor (ν^4/ν_0^4) to avoid unrealistic values of opacity in the far wings of the strong lines.

Medium lines have $10^{-5} \leq S < 0.025$ and are included only if they fall within 100 Doppler half-widths of a particular sampling wavelength. Their contribution is computed with a Voigt profile and is included whenever equation (3) is satisfied. The

© American Astronomical Society • Provided by the NASA Astrophysics Data System

1994ApJ...437..879A

definitions of strong, medium, and weak lines and the criterion in equation (3) were all determined so that the effect on the final result (compared to treating all lines at all wavelengths) was less than 0.5%.

Out of the total of 8,216,994 atomic lines listed in Table 3, we treat 558 in the strong line and 21,985 in the medium line formalisms described above. All other lines are considered as weak lines, with Doppler profiles. Using a procedure first suggested by Jøgensen (1990), an opacity table is constructed for each species which has more than 10,000 weak lines. In each opacity table, the temperature-dependent portion of the opacity of the species is pretabulated at each sampling frequency. All that is required to compute the opacity of this species at a given temperature-density point is to interpolate in this table for the proper temperature and multiply by the number density of the species computed by the EOS. This procedure introduces errors of less than 0.5%, decreases the computation time by a factor of 5, and decreases the memory requirements by a factor of 20.

Hydrogen lines are treated separately using Griem's (1960, 1967) formulation of the Stark broadening, as computed by subroutines from K70. While this treatment is not sufficient for line profile analysis, it is sufficient for the computation of mean opacities where the detailed wavelength dependence of the line absorption is averaged out.

3.2. *Scattering*

Electron scattering and Rayleigh scattering from H I, He I, and H_2 are computed from the standard formulae by subroutines taken from K70. All spectral lines are assumed to be in pure absorption. Scattering by dust grains will be discussed in § 3.4.

3.3. *Molecular Absorption*

Bound-bound absorption by molecules becomes a noticeable source of opacity at temperatures as high as 5000 K (especially at high densities) and a dominant source for temperatures below 2500 K. All molecular absorption is computed monochromatically. A variety of molecules are considered to account for as much of the total absorption as possible for a wide variety of chemical compositions. Jørgensen (1994b) has demonstrated that it is extremely important to include as many weak lines as possible in order to accurately predict the emergent spectrum from a stellar atmosphere model. He has shown that, in the case of H_2O, there are large changes in photospheric structure when the completeness factor is increased from 90% to 95% and noticeable changes in structure occur until 98% of the total theoretical molecular absorption is included. Because the Rosseland mean opacity is a harmonic mean, and therefore emphasizes those wavelengths with the smallest monochromatic opacity at wavelengths where the weighting function is significant, it is also important to include as many weak lines as possible in this calculation. The discussion of Figure 15 in § 4.2 presents another dramatic example of this point. Therefore, an attempt has been made to utilize the most extensive line lists available for all the significant molecular absorbers.

Table 4 lists the molecular absorbers considered, along with the source of the data utilized for each. All molecular lines are computed with Doppler profiles (with turbulent velocity of 2 km s^{-1}, as described in § 3.1.2), and are included if they fall within 4 Doppler half-widths of a sampled frequency. A total of 59 million lines are included in the molecular archive. The opacity of molecules which contain carbon are computed with lines of both C^{12} and C^{13}, with the ratio $C^{12}/C^{13} = 90$ set at the solar value (Anders & Grevesse 1989). The Ti isotopes included in the TiO lines have the solar abundance ratios $Ti^{46}:Ti^{47}:Ti^{48}:Ti^{49}:Ti^{50} = 0.0825:0.0745:0.737:0.054:0.052$. The Zr isotopes included in the ZrO lines have the solar abundance ratios $Zr^{90}:Zr^{91}:Zr^{92}:Zr^{94}:Zr^{96} = 0.52:0.11:0.17:0.17:0.03$. The oscillator strengths for ZrO have been updated by the recent laboratory analysis by Littleton, Davis, & Song (1993).

TABLE 4

MOLECULAR OPACITY SOURCES

Molecule	Number of lines	Source of Data
CO	37720	Goorvitch & Chackerian 1994
H_2O	20000000	Jørgensen & Jensen 1993
		Jørgensen, Jensen, & Sørensen 1994
TiO	12312080	Jørgensen 1994a
CN (Red system)	2200000	Jørgensen & Larsson 1990
CN (Violet B-X system)	323818	Kurucz 1991
SiO	14401	Tipping & Chackerian 1981
H_2-H_2 (collision induced)		Borysow & Frommhold 1990
		Zheng & Borysow 1994
H_2-He (collision induced)		Borysow, Frommhold & Moraldi 1989
		Borysow & Frommhold 1989
CH	61856	Sharp 1984
C_2	1494062	Sharp 1984
HCN	10000000	Jørgensen et al. 1985
C_2H_2	10000000	Jørgensen 1993
ZrO	311735	Littleton & Davis 1985
YO	1197	Littleton 1987
MgH	9396	Sharp 1981
SH	1644	Sharp 1981
HCl	3829	Sharp 1981
HF	1295	Sharp 1981
NH	613	Bell 1979
OH	801	Bell 1979
AlH	7249	Tipping 1987
SiS	592	Lopez Piñeiro, Tipping, & Chackerian 1987b
CS	35471	Lopez Piñeiro, Tipping, & Chackerian 1987a

© American Astronomical Society • Provided by the NASA Astrophysics Data System

1994ApJ...437..879A

The free-free absorption of H_2^- is included utilizing the results of Dalgarno & Lane (1966). The bound-free and free-free absorption of H_2^+ is computed by a subroutine from K70.

3.4. *Absorption and Scattering by Dust Grains*

The absorption and scattering by dust grains is treated by Rayleigh scattering theory for a continuous distribution of ellipsoids (Bohren & Huffman 1983). Since our treatment of this method has been discussed extensively elsewhere (Alexander & Ferguson 1994), it will only be briefly summarized here. The continuous distribution of ellipsoids model assumes that the dust particles are triaxial ellipsoids, with all mathematically possible shapes represented by equal probabilities. All possible orientations of the ellipsoids are also considered to be equally probable. This double averaging over shape and orientation allows the complex polarizability of the particle ensemble to be computed from the dielectric function of the material in the grain. Once the polarizability is known, the absorption and scattering efficiencies can be calculated from Rayleigh theory. At the very shortest wavelengths (far from the peak of the weighting function), the Rayleigh approximation breaks down and is replaced by a Mie calculation for spherical particles. Iron grains are treated entirely with the Mie theory for spherical particles because the Rayleigh criterion $(2\pi a/\lambda|m| \ll 1$, where a is the grain radius and m is the complex index of refraction) is violated for most grain sizes even for wavelengths near the peak of the weighting function due to the large values of the index of refraction.

The sources for the optical properties of the dust grains included in this study, in the form of complex indices of refraction, are presented in Table 5. These optical properties have been selected as the most representative of the species likely to be present in warm, dusty gases in typical astrophysical environments. It is assumed that the optical constants for cool oxygen-rich silicates (Ossenkopf, Henning, & Mathis 1992) represent the optical properties of all the common silicates which may condense. Other trace condensates are not included, even though they may significantly affect the opacity if no other materials have condensed, because we lack data for them. The omission of common low-temperature condensates such as FeS, Fe_3O_4, and (ultimately) H_2O in our calculations sets a practical lower limit of about 700 K for the applicability of our results (Grossman 1972). Both oxygen-rich and carbon-rich mixtures are permitted, although results for only the oxygen-rich case will be discussed here.

The size distribution of the grains is assumed to follow the power law determined from observations of interstellar reddening (Mathis, Rumple, & Nordsiek 1977) with radii between 0.005 and 0.25 μm for all grain species. If the power law with exponential decay size distribution recently obtained by Kim, Martin, & Hendry (1994) is used instead, the Rosseland mean opacities in the standard composition are increased by about 15%. However, the larger particles allowed in this distribution violate the Rayleigh criterion for a wide range of wavelengths near the peak of the weighting function.

TABLE 5

SOURCES OF OPTICAL CONSTANTS FOR DUST GRAINS

Grain Species	Source of Optical Constants
Cool oxygen-rich silicates.....	Ossenkopf, Henning, & Mathis (1992)
Iron	Ordal et al. (1988)
	Johnson & Christy (1974)
Amorphous carbon	Rouleau & Martin (1991)
Silicon carbide	Pégourié (1988)

4. RESULTS

Tables of Rosseland and Planck opacities have been computed for a wide range of chemical compositions. Our standard tables cover the temperature range from log $T = 4.10$ to log $T = 2.85$. The densities covered by our standard tables range from log $R = -7.0$ to log $R = +1.0$. These values of R cover the density range 10^{-13} to 10^{-5} g cm^{-3} at 10,000 K and the density range 10^{-16} to 10^{-8} g cm^{-3} at 1000 K. These table limits are required because of the exclusion of both high-temperature absorbers and the wide variety of grain species which form at progressively lower temperatures. Somewhat higher or lower densities could be included if they are important for specialized applications.

An example of our results for one composition ($X = 0.70$ and $Z = 0.02$ with the Grevesse 1991 mix of heavy elements is shown in Table 6. It has been our experience that investigators who utilize these tables require unique combinations of temperature-density coverage, chemical composition, and table format. Instead of attempting to publish or make available electronically a large set of general tables, we will instead offer to compute upon request tables for any set of circumstances within the constraints permitted by our program. This effort is possible through the support of NSF grant AST-9217946. Requests for tables should be sent to the first author at the internet address: dra@twsuvm.uc.twsu.edu. In addition to being able to compute tables for standard chemical compositions, we are especially interested in preparing tables with unusual abundances to model specialized astrophysical phenomena.

4.1. *Analysis of Opacity Results*

The effects of changing metallicities is demonstrated in Figure 1 for a slice through the table at log $R = -3.0$. As expected, the higher the metallicity, the higher the opacity. More specifically, the following observations can be made. For temperatures above about 5000 K, the opacities are dominated by hydrogenic absorption and are little affected by composition. For temperatures between 5000 and 2500 K the opacities are still dominated by hydrogenic absorption (principally, H^- and Rayleigh scattering), but the metals make an increasingly

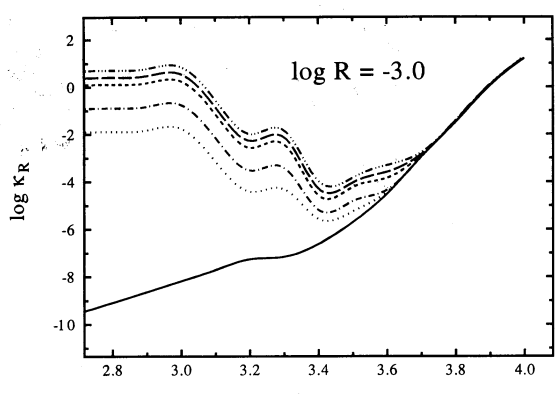

FIG. 1.—The Rosseland mean opacity as a function of temperature for different chemical compositions. From the bottom, the abundance of the metal is $Z = 0.9$, 0.0001, 0.001, 0.01, 0.02, and 0.04. The value of R is held constant at 0.001 and $X = 0.70$ for each curve.

© American Astronomical Society • Provided by the NASA Astrophysics Data System

© American Astronomical Society • Provided by the NASA Astrophysics Data System

1994ApJ...437..879A

TABLE 6

MASTER GRID OF ROSSELAND OPACITIES (GREVESSE 1991 MIX WITH $X = 0.70$ AND $Z = 0.02$)

log T	log R																
	-7.0	-6.5	-6.0	-5.5	-5.0	-4.5	-4.0	-3.5	-3.0	-2.5	-2.0	-1.5	-1.0	-0.5	0.0	0.5	1.0
4.100	-0.493	-0.479	-0.439	-0.342	-0.147	0.160	0.570	1.023	1.476	1.887	2.217	2.453	2.618	2.742	2.851	2.966	3.096
4.050	-0.509	-0.497	-0.447	-0.325	-0.097	0.233	0.650	1.078	1.467	1.773	1.987	2.135	2.247	2.344	2.447	2.570	2.717
4.000	-0.529	-0.498	-0.429	-0.285	-0.054	0.271	0.646	0.991	1.257	1.441	1.571	1.674	1.768	1.871	1.991	2.137	2.311
3.950	-0.521	-0.482	-0.405	-0.267	-0.062	0.198	0.447	0.643	0.784	0.893	0.990	1.092	1.205	1.337	1.490	1.671	1.880
3.900	-0.510	-0.475	-0.414	-0.326	-0.223	-0.126	-0.046	0.029	0.108	0.201	0.313	0.446	0.598	0.770	0.963	1.182	1.425
3.850	-0.524	-0.527	-0.546	-0.593	-0.657	-0.713	-0.742	-0.725	-0.655	-0.539	-0.387	-0.210	-0.016	0.196	0.425	0.674	0.952
3.800	-0.669	-0.790	-0.943	-1.111	-1.275	-1.412	-1.496	-1.500	-1.418	-1.268	-1.075	-0.862	-0.631	-0.386	-0.120	0.174	0.500
3.750	-1.112	-1.321	-1.537	-1.751	-1.952	-2.122	-2.229	-2.241	-2.147	-1.978	-1.757	-1.509	-1.235	-0.933	-0.593	-0.213	0.181
3.700	-1.765	-1.997	-2.224	-2.443	-2.644	-2.812	-2.921	-2.932	-2.836	-2.647	-2.387	-2.067	-1.690	-1.273	-0.851	-0.450	-0.078
3.650	-2.522	-2.742	-2.951	-3.147	-3.323	-3.465	-3.546	-3.530	-3.387	-3.113	-2.735	-2.307	-1.875	-1.469	-1.098	-0.759	-0.446
3.600	-3.297	-3.478	-3.642	-3.783	-3.889	-3.939	-3.912	-3.783	-3.545	-3.220	-2.853	-2.485	-2.136	-1.814	-1.509	-1.214	-0.926
3.550	-3.940	-4.033	-4.086	-4.100	-4.080	-4.030	-3.945	-3.817	-3.640	-3.420	-3.167	-2.896	-2.617	-2.330	-2.027	-1.718	-1.420
3.500	-4.182	-4.169	-4.147	-4.121	-4.102	-4.094	-4.086	-4.059	-3.996	-3.883	-3.695	-3.413	-3.019	-2.521	-1.979	-1.498	-1.169
3.450	-4.203	-4.207	-4.231	-4.274	-4.333	-4.404	-4.469	-4.503	-4.465	-4.279	-3.870	-3.270	-2.608	-2.014	-1.596	-1.363	-1.245
3.400	-4.387	-4.460	-4.550	-4.650	-4.745	-4.812	-4.818	-4.688	-4.319	-3.700	-2.990	-2.351	-1.885	-1.625	-1.507	-1.454	-1.428
3.350	-4.796	-4.896	-4.971	-5.004	-4.974	-4.832	-4.479	-3.881	-3.174	-2.529	-2.055	-1.802	-1.698	-1.658	-1.641	-1.631	-1.623
3.300	-5.133	-5.117	-5.060	-4.894	-4.515	-3.903	-3.194	-2.559	-2.134	-1.939	-1.869	-1.844	-1.834	-1.828	-1.825	-1.822	-1.820
3.250	-5.131	-4.888	-4.409	-3.724	-3.012	-2.463	-2.186	-2.088	-2.057	-2.045	-2.040	-2.037	-2.036	-2.034	-2.033	-2.032	-2.029
3.200	-4.011	-3.281	-2.702	-2.420	-2.329	-2.301	-2.291	-2.288	-2.285	-2.284	-2.284	-2.285	-2.285	-2.284	-2.284	-2.280	-0.881
3.150	-2.496	-2.448	-2.434	-2.429	-2.428	-2.427	-2.427	-2.427	-2.428	-2.428	-2.429	-1.133	-0.936	-0.756	-0.653	0.026	0.413
3.100	-2.423	-2.423	-2.423	-2.424	-2.424	-2.425	-1.346	-1.092	-0.862	-0.269	0.060	0.143	0.354	0.505	0.593	0.626	0.657
3.050	-2.427	-2.427	-1.203	-0.957	-0.479	-0.045	0.156	0.257	0.351	0.449	0.532	0.569	0.594	0.599	0.600	0.601	0.601
3.000	-0.263	-0.091	0.111	0.245	0.329	0.414	0.488	0.529	0.546	0.547	0.548	0.548	0.548	0.548	0.548	0.548	0.548
2.950	0.254	0.320	0.398	0.466	0.499	0.501	0.502	0.502	0.502	0.502	0.502	0.502	0.502	0.502	0.502	0.502	0.502
2.900	0.423	0.458	0.460	0.461	0.462	0.462	0.462	0.462	0.462	0.462	0.462	0.462	0.462	0.462	0.462	0.462	0.462
2.850	0.429	0.430	0.430	0.430	0.430	0.430	0.430	0.430	0.430	0.430	0.430	0.430	0.430	0.430	0.430	0.430	0.430

1994ApJ...437..879A

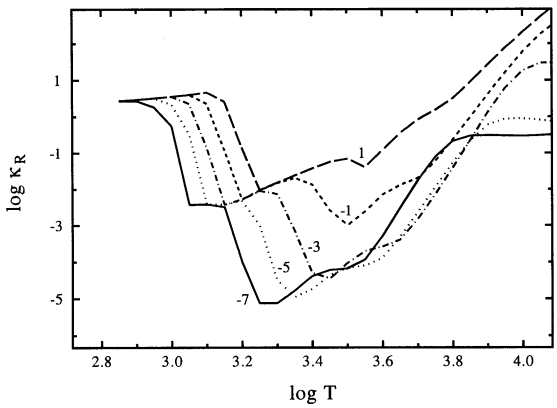

FIG. 2.—The Rosseland mean opacity as a function of temperature for the solar composition. Each curve is labeled with the value of log R.

important contribution to the number of free electrons (as the degree of hydrogen ionization decreases) as the metallicity is increased. The sharp rise in the opacity at 2500 K signals the emergence of H_2O as a dominant absorber. Grain condensation at about 1500 K creates an even larger increase in the total absorption.

The opacities of the master grid in Table 6 are plotted in Figure 2. The effect of grain opacity is seen on the left. As the density increases, the condensation temperature of grains increases and, as a result, the steep rise in the opacity below 2000 K gradually shifts to higher temperatures with increasing density. The plateau in the opacity between 1500 and 3200 K is the result of molecular absorption, mostly H_2O. This bump also moves to higher temperatures with increasing density under the influence of the law of mass action. At the highest density H_2O is the major contributor to the Rosseland mean for all temperatures below 3200 K, until grain condensation occurs at about 1600 K. At 5000 K Rayleigh scattering dominates at low densities while H^- dominates at higher densities. At this and all higher temperatures, absorption and scattering by hydrogen and H^- dominates the opacity with only minor contributions from the atomic lines.

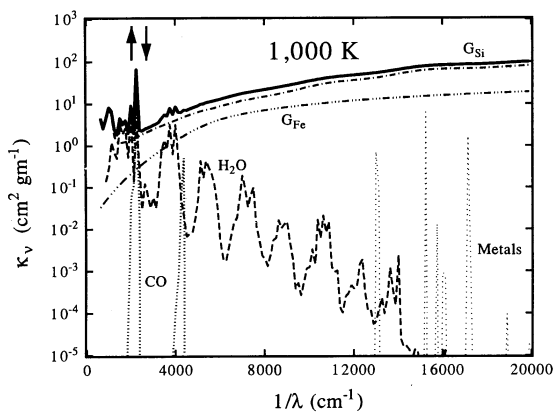

FIG. 3.—The monochromatic absorption coefficient of selected species at 1000 K and $R = 0.001$. Line sources have been smoothed with a Gaussian filter with a half-width of 15 cm^{-1}. The symbols are defined as: G_{Si} = silicate grains; G_{Fe} = iron grains; metals = atomic lines; H_2O = water vapor; and CO = carbon monoxide. The heavy solid line represents the total opacity. The upward pointing arrow denotes the wavelength of the maximum of the Planck function, while the downward pointing arrow shows the location of the maximum of the Rosseland weighting function.

The frequency dependence of some of the important absorbers is demonstrated in Figures 3–6. In each of these figures, the opacities have been smoothed with a Gaussian function with a half-width of 15 cm^{-1} so that the extreme variability of the line absorbers computed with opacity sampling is somewhat smoothed out. (It should be emphasized that this smoothing was done only for purposes of these figures, and

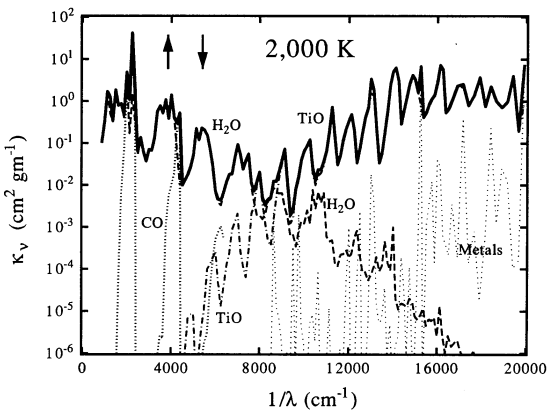

FIG. 4.—Same as Fig. 3, except at 2000 K. Titanium oxide (TiO) has been added.

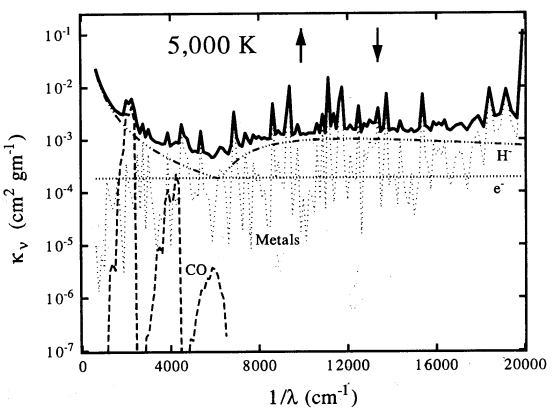

FIG. 5.—Same as Fig. 3, except at 5000 K. The negative hydrogen ion (H^-), hydrogen bound-free and free-free (H), and Rayleigh scattering from hydrogen (R_H) have been added.

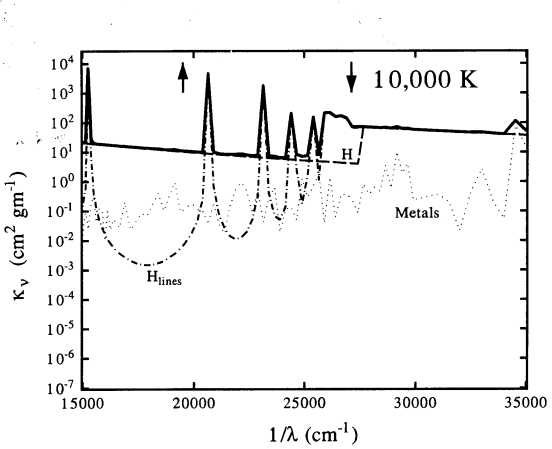

FIG. 6.—Same as Fig. 3, except at 10,000 K. Hydrogen lines (H_{lines}) have been added.

© American Astronomical Society • Provided by the NASA Astrophysics Data System

1994ApJ...437..879A

was not used in any of the Rosseland opacity calculations.) To remind the reader of the importance of the weighting function used in computing mean opacities, the downward pointing arrow in each figure denotes the maximum of the weighting function for Rosseland mean calculations ($\partial B_\nu/\partial T$), while the upward pointing arrow denotes the maximum of the weighting function of the Planck mean calculations (B_ν). Each figure presents results for the density parameter (log R) value of -3.0.

At 1000 K the opacity at all but a few long wavelengths is controlled by the opacity of silicate and iron grains. Note that carbon and SiC grains do not form unless the C/O abundance ratio is very close to 1.0. H_2O and CO affect the total opacity at a few wavelengths; no other opacity source affects the total opacity in the region near the peaks of the weighting functions.

At 2000 K the total opacity is dominated by molecules, principally H_2O and TiO. Atomic lines and CO lines are important at a few wavelengths. While not shown here, continuous sources such as Rayleigh scattering from H and H_2 and H^- absorption are important at individual wavelengths where no molecule happens to have a strong absorption feature, even though their average absorption coefficient is only about 10^{-3} cm^2 g^{-1} or less in this spectral region. This effect is a result of the harmonic nature of the Rosseland average. For example, the Rosseland mean would be reduced by almost a factor of 3 if the H^- opacity were left out.

At 5000 K the atomic lines and H^- dominate the total opacity in the region around the peaks of the weighting functions. It is again important to have the continuous absorbers as a floor under the line sources. The total opacity would still be reduced by a factor of 3 if the H^- absorption was excluded.

At 10,000 K, hydrogen (bound-free, free-free, and lines) dominates the total opacity, with metals contributing at a few frequencies. Hydrogen lines are only a 20% factor in the Rosseland mean at this temperature despite their prominence in the spectrum.

The consequences of these effects from individual absorbers on the Rosseland mean can be examined in Figure 7. In addition to showing the total Rosseland opacity at a fixed value of R, this figure also shows the Rosseland opacity of all absorbers *except one* for each of the major absorbers. These partial opacity curves are labeled with the excluded absorber in each case. Since the vertical scale is greatly compressed, only those absorbers which affect the overall Rosseland average by at least a factor of 2 are shown. As expected, grains and H_2O have an overpowering effect at low temperatures while hydrogen bound-free and free-free absorption produce more than an order of magnitude effect at high temperatures. No other opacity source produces as much as half an order of magnitude effect at any temperature for this value of R. However, at other values of R some additional opacity sources can be dominant. For example, at low densities scattering dominates the opacity at all temperatures above the grain condensation temperature. At high densities H^- is more significant because of the enhanced level of ionization present.

Because of the wide availability of atomic opacities, it is important to know the limits of their applicability. Figure 8 demonstrates the consequences of neglecting molecules both as opacity sources and in the equation of state. At 4000 K the difference between the opacity without any molecular effects and our standard opacity reaches a maximum value of 38% at intermediate densities. At 5000 K the maximum differential is only 12%, too low to show on the scale of this figure. As the temperature is decreased, the differential grows systematically and become significant at progressively lower densities.

The Planck mean opacity is defined as

$$\kappa_P = \frac{\int_0^\infty \kappa'_\nu B_\nu \, d\nu}{\int_0^\infty B_\nu \, d\nu}, \tag{4}$$

where κ'_ν is the monochromatic opacity including only absorption (not scattering) processes. Because the derivation of the diffusion approximation (and the Rosseland mean) assumes that the radiation field is isotropic, its use in optically thin media is not strictly valid. However, the ratio of the Rosseland mean to the Planck mean opacity provides important information about the appropriateness of solving the radiative transport via the diffusion approximation in optically thin media (Alexander & Ferguson 1994, and references therein). When the ratio is close to unity, the diffusion approximation will produce a reliable estimate of the thermal structure of the medium even when it is optically thin. However, when the ratio deviates significantly from unity, structures of optically thin media obtained from the diffusion approximation may be unreliable.

Figure 9 helps us determine in which temperature-density regions the diffusion approximation can be safely applied to

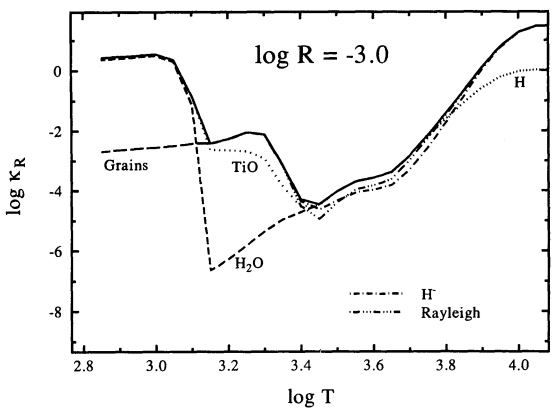

FIG. 7.—The Rosseland mean opacity as a function of temperature for $R = 0.001$. The solid line represents the total Rosseland mean opacity for the solar composition. All other lines represent the Rosseland mean opacity for all sources except the source labeled. For example, the line labeled H_2O is the Rosseland mean opacity of all species except water vapor.

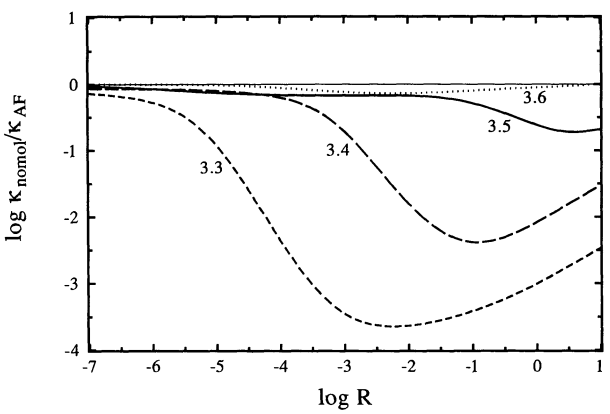

FIG. 8.—The ratio of the opacity without any molecular effects in either the opacity calculation or in the equation of state to the standard opacity from the master grid. The curves are labeled with the value of log T.

© American Astronomical Society • Provided by the NASA Astrophysics Data System

1994ApJ...437..879A

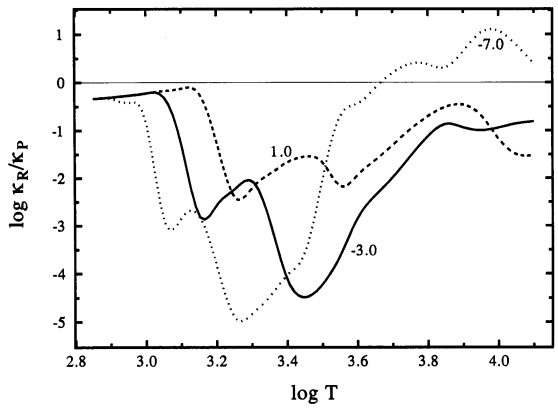

FIG. 9.—The ratio of the Rosseland mean opacity to the Planck mean opacity as a function of temperature. Each curve is labeled with the value of log R for that curve. A reference line for a ratio of 1.0 is included.

optically thin media. When the opacity is dominated by the opacity of grains, the ratio of the mean opacities is always close to one. For temperatures above about 6000 K, where the opacity is dominated by continuous absorbers such as hydrogen bound-free and free-free, the ratio is again reasonably close to one. In those conditions where the opacity is dominated by line sources the ratio of opacities deviates dramatically from unity. Under these circumstances the use of the diffusion approximation to obtain the thermal structure of optically thin media becomes highly suspect. There is, of course, no error introduced in using a Rosseland optical depth as a depth indicator in a model photosphere obtained from the solution of the non-gray equation of radiative transfer.

4.2. *Comparison to Other Results*

Figure 10 compares our opacities to those obtained by the OPAL project (Rogers & Iglesias 1992), where each curve is labeled by the temperature in thousands of kelvins. It is not surprising than our opacities are smaller than the OPAL results at high temperatures because of the neglect of high-temperature absorbers in our computation. For example, at a temperature of 14,000 K and log $R = -3.0$, the second ionization stage of many of the heavy elements has a significant population, but we have included only the strongest lines of those species. This limitation sets a practical upper limit for our results at about 12,500 K. The agreement between our results and the Opal results is very good at 10,000 K, never exceeding 5% at any density and averaging better than 3%.

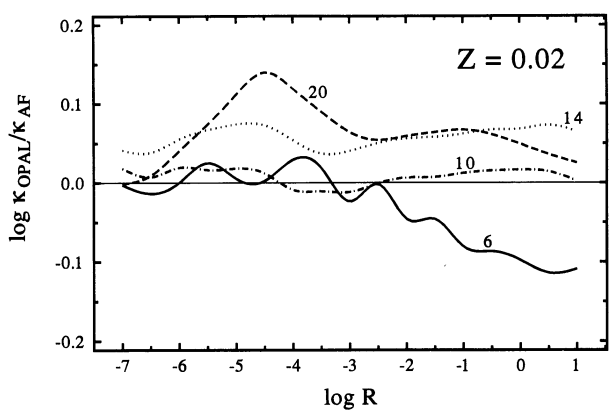

FIG. 10.—The ratio of the Rosseland mean opacity obtained by OPAL to the results of the present study as a function of R for the solar composition. Each curve is labeled by the temperature in thousands of kelvins.

At the lowest temperature included in the OPAL tables, our opacities become somewhat higher than theirs at the highest densities, reaching a maximum differential of 0.109 dex at $R = 10$. The differential at this point is reduced only by 0.014 dex if the effects of molecules are removed from our calculations (molecules are not included in the OPAL calculation). A detailed comparison of the results of our EOS calculation with those of OPAL (Iglesias 1993) at 6000 K and log $R = 1.0$ shows excellent agreement. Since we both use the same cross section data for H^-, most of the remaining difference in our opacities must be due to differences in the treatment of the only other significant absorber, atomic lines. One difference in our treatment of atomic lines is that we treat each element explicitly for all elements up to copper, while OPAL considers only 12 heavy elements. This simplification of the EOS removes the veil of millions of weak lines of the excluded elements, even though the abundance of the neighboring elements is adjusted to compensate for the excluded elements. Jøgensen (1994b) has shown that a veil of weak lines can be critically important to the structure of cool stellar atmospheres (see discussion in § 3.2). As is the case for Rosseland mean calculations, the radiative transfer in a stellar atmosphere is strongly affected by any wavelengths near the flux maximum which have very low opacity. While the OPAL treatment of elements has been shown to be accurate at higher temperatures (Iglesias & Rogers 1991), the validity of this approximation at lower temperatures has not been demonstrated. Indeed, when we use their abundances instead of the full set of elements, the differential is reduced by 0.022 dex at this point. Almost all of this effect is the result of the loss of the veil of weak lines of the excluded elements. The electron balance (which controls the H^- opacity) is hardly affected since the abundance of neighboring elements with nearly the same ionization potential is adjusted for the excluded elements.

Still another factor which affects the comparison at this point is that we have assumed a turbulent velocity of 2 km s^{-1} (characteristic of a stellar photosphere) in computing the Doppler broadening of the atomic lines while OPAL did not include turbulence in their calculation of Doppler broadening. Their assumption of no turbulence is reasonable at the higher temperature which are their primary interest because thermal velocities will be greater than any reasonable turbulent velocity. However, at the temperatures of interest here, turbulent velocities characteristic of a stellar photosphere contribute significantly to the Doppler broadening of the lines. Removing the turbulent velocity reduces the differential at this point by 0.008 dex.

Finally, if we limit the evaluation of strong lines (as defined in § 3.1.2) to 100 Doppler half-widths of line center, the differential is reduced by 0.009 dex. These four factors account for half of the differential at this point; neglecting them brings our values into reasonable agreement (0.057 dex) with OPAL results.

The influence of the metals is eliminated in Figure 11, which compares our results to the OPAL results for the composition $X = 0.70$ and $Z = 0$. The ratio of opacities is much closer to unity for most temperatures and densities in this figure. The rms average deviation for all table points contained in the range covered by the figure is less than 5%.

© American Astronomical Society • Provided by the NASA Astrophysics Data System

1994ApJ...437..879A

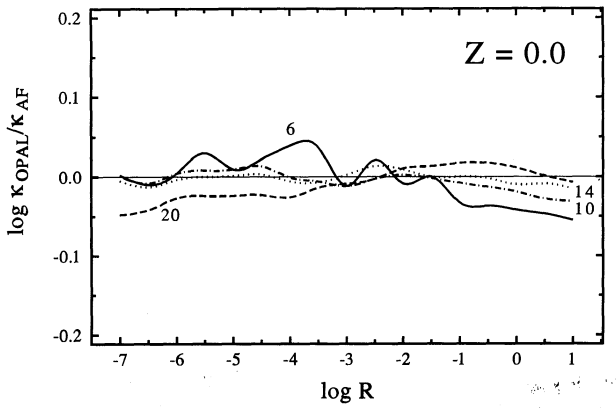

FIG. 11.—Same as Fig. 10, except for the zero metallicity case

Lenzuni et al. (1991) have also computed metal-free opacities. We compare our results to theirs in Figure 12. Data points outside the normal density range for our tables (log $R > 1.0$) are represented as dotted lines in this figure. For densities in our normal range, our opacities generally agree quite well with the results of Lenzuni et al. (1991), with an rms difference of only 8%. At 5000 K most of the difference at high density is the result of our adoption of more accurate values for the partition function for H_3^+, which were not available at the time of their study. At 1000 K and 3000 K the differences at high density are the result of using different data for collision-induced absorption by H_2–H_2 pairs. Lenzuni et al. include estimated data for the overtone and double vibration bands which we have chosen not to include. Since these bands fall near an opacity minimum, they significantly influence the Rosseland mean even though they are a hundred times weaker than the fundamental (cf. Fig. 3 of Lenzuni et al.). Nonideal effects in the EOS would further alter our results for densities greater than 10^{-2} g cm^{-3} (Lenzuni & Saumon 1992).

Our results are compared to those of the OP project in Figure 13, with each curve labeled by log T. This plot shares many of the features of Figure 10. Again, our opacities underestimate the total opacity at high temperatures due to the neglect of high-temperature atomic species. At intermediate temperatures, the agreement is very good. For example, at

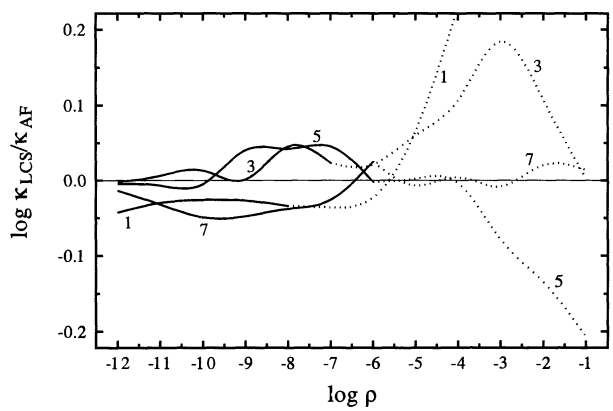

FIG. 12.—The ratio of the Rosseland mean opacity obtained by Lenzuni et al. (1991) to the results of the present study as a function of density for the zero metallicity case. Each curve is labeled with the temperature in thousands of kelvins. Dotted curves show the extension of the comparison beyond the normal range of our tables.

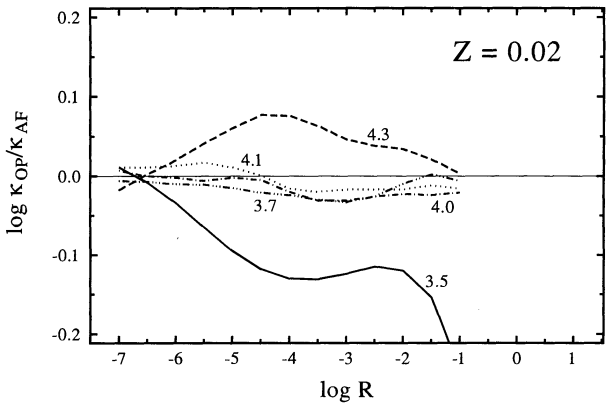

FIG. 13.—The ratio of the Rosseland mean opacity obtained by OP to the results of the present study as a function of R for the solar composition. Each curve is labeled with the value of log T.

10,000 K the rms deviation is less than 5%. At the lowest temperature included in the OP results, the consequences of OP having neglected molecules becomes quite noticeable. As the density is increased at 3200 K the contribution of molecules becomes more and more significant. At the highest density included in their table, CO, H_2O, and TiO each make a contribution of at least 25% to the Rosseland mean, i.e., the Rosseland mean is reduced by at least 25% from its total value when any one of these opacity sources is removed from the calculation. If all molecules are removed from the computation, the Rosseland mean is reduced by more than 60% at this point, and then our result agrees well with the OP result.

Figure 14 presents the comparison between our results and the OP results for the metal-free case. The agreement between the results is strikingly good. In the temperature range of 12,000–5000 K, the rms difference is less than 5%.

The present results are compared to our previous compilations (AJR) in Figure 15, where the curves are labeled by log T. Note that a different vertical scale is required here to show the rather large differences in opacities which occur at low temperatures. The increase in the opacity in the present study at 1000 K is the result of our use of the continuous distribution of ellipsoids formulation for computing the opacity of the grains, as well as updated optical constants for the grains. The effects of the continuous distribution of ellipsoids formulation are discussed elsewhere in more detail (Alexander & Ferguson 1994).

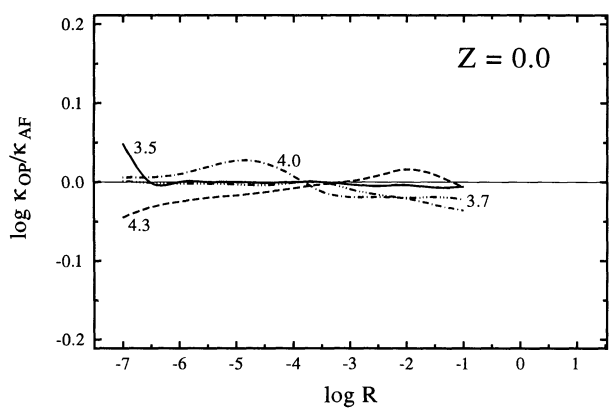

FIG. 14.—Same as Fig. 13, except for the zero metallicity case

© American Astronomical Society • Provided by the NASA Astrophysics Data System

1994ApJ...437..879A

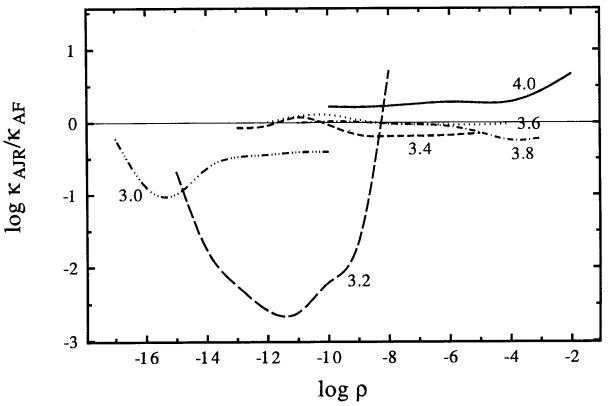

FIG. 15.—The ratio of the Rosseland mean opacity obtained by Alexander et al. (1983) to the results of the present study as a function of density. Each curve is labeled by the value of log T.

The very large changes seen at log $T = 3.2$ are the result of a subtle effect in the computation of a Rosseland mean. AJR computed the opacity of water vapor using the straight mean data of Auman (1967). Because those data have a long wavelength cutoff of 850 cm^{-1}, the only opacity at longer wavelengths is a very small contribution from continuous sources. At higher temperatures the consequence of this deficiency in the data is not large because the peak of the Rosseland weighting function is at much shorter wavelengths. At this lower temperature, however, the wavelengths with no water vapor opacity have become weighted by the Rosseland weighting function, which caused the AJR calculation to significantly underestimate the total opacity.

More modest changes are seen in the results for higher temperatures. Nevertheless, it must be remembered that the vertical scale has been greatly compressed here. At log $T = 3.4$, changes in the opacity by a factor of 50% or more are not uncommon due to the improvement in the spectral data for H_2O. At intermediate temperatures, the differences are due primarily to the significant expansion of the atomic line list used here. The decrease in the opacity at 10,000 K is the result of a correction in the H^- opacity introduced in Alexander, Augason, & Johnson (1989).

Finally, the results of the present study are compared to several recent investigations of low-temperature opacities in Figure 16. Some of these computations were based upon slightly different solar compositions from that assumed here. These slight abundance variations can cause differences in the Rosseland opacities as great as 0.1 dex, or about twice the thickness of the lines in the figure. There is good convergence of the results for temperatures above 5000 K. The OPAL results are not shown because they are indistinguishable from our results at this scale over the entire range of temperatures covered in those tables. Since we use virtually identical atomic opacity sources as Kurucz (1992), we would expect to agree very closely with results obtained by him at temperatures where only atomic sources contribute to the opacity.

The effects of different treatments of the H_2O spectrum are evident for temperatures between 1500 and 2800 K. Plez (1992), Sharp (1992), and Allard et al. (1994) all underestimate the contribution of water vapor to the Rosseland mean due to the use of incomplete line lists. In the context of stellar atmospheric structure, Jørgensen (1994b) has conclusively shown that at least 98.5% of the total band strength of water vapor must be included to obtain convergence of the structure. This requires the use of 20 million lines, more than twice as many as included in the other studies. The straight mean results of Allard et al. somewhat overestimate the contribution of water vapor at the lowest temperatures. With decreasing temperature the population of moderately excited levels decreases and more wavelengths with low opacity occur, which makes the correct treatment of individual lines more significant.

Weiss et al. (1990), who include unspecified molecular absorbers, significantly overestimate the opacity below 5500 K. The preliminary results of Bell (1994) are significantly lower than ours for temperatures below 2500 K because his H_2O line list did not include any data longward of 5 μm. If we remove H_2O from our calculation for wavelengths longer than 5 μm, our result is reduced by more than two orders of magnitude at 2000 K and agrees reasonably well with his result. The OP results are indistinguishable from Bell's results down to the limit of their tables at 3160 K.

The current work agrees well in both condensation temperature and total grain opacity with the work of Pollack et al.

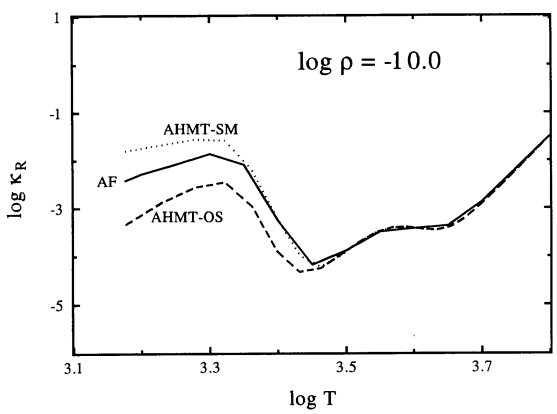

FIG. 16*a*

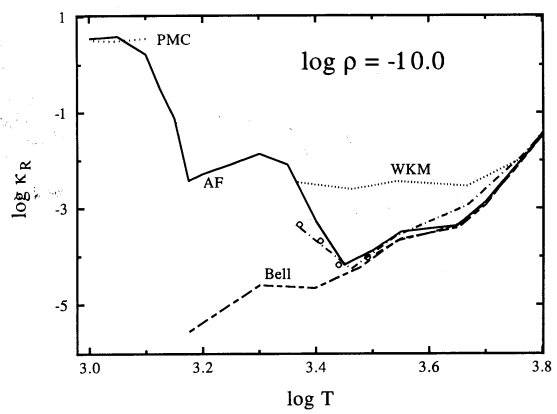

FIG. 16*b*

FIG. 16.—(*a*) The results of the present study (labeled AF) compared to results from Allard et al. (1994). The curve labeled AHMT–OS is slightly revised data from Allard et al. obtained by opacity sampling the H_2O spectrum. The curve labeled AHMT–SM represents slightly revised data from Allard et al. based upon straight mean H_2O data. (*b*) The Rosseland mean opacity obtained in several investigations as a function of temperature. Curves are labeled as follows: WKM = Weiss et al. (1990); PMC = Pollack et al. (1985); Bell = preliminary results from Bell (1994); and AF = the present study. The open circles show values extracted from the model atmospheres of Plez (1992). The unlabeled dot-dash curve shows the results of Sharp (1992).

© American Astronomical Society • Provided by the NASA Astrophysics Data System

1994ApJ...437..879A

(1985). For the temperatures covered here, the results of Pollack et al. (1994) are indistinguishable from their earlier results. It is encouraging that grain opacities computed with such radically different assumptions and data agree so well.

5. CONCLUSIONS

From comprehensive opacity sampling calculations, Rosseland and Planck mean opacities have been computed over the temperature range 12,500–700 K for a range of different chemical compositions. The effects of atomic, molecular, and solid particulate absorbers and scatterers are included. Tables will be computed by the authors for any requested composition and combination of temperatures and densities within the constraints discussed above.

All mean opacities are computed from monochromatic opacities. The effects of more than 68 million lines have been included in the computation, along with 19 continuous sources and four dust grain species. It is especially important that a large number of weak lines are included because the inverse nature of the Rosseland average makes it very susceptible to individual frequencies which have very little opacity.

The results presented here agree well with other recent opacity tabulations for temperatures above 5000 K. At progressively lower temperatures, molecules play an increasingly more important role, and those computations which ignore molecular effects underestimate the total opacity. At 3000 K and high densities the triatomic molecule H_2O is an important opacity source. At about 1500 K (depending on the density) dust grains form and completely dominate the total opacity for lower temperatures.

It must be emphasized that all results reported here assume that all species are in complete chemical equilibrium, the abundance ratios of the elements heavier than helium follow the solar values, and the size distribution of the grains follows the distribution law determined for interstellar grains. These assumptions are required in order to obtain generalized tabulations which can be utilized to model a wide range of situations. Violations of these assumptions are likely under certain circumstances. Effects of possible departures from LTE on molecular opacities has been recently reviewed by Johnson (1994). Dust formation within the photospheres of cool giant stars is also probably not in chemical equilibrium (Dominik, Sedlmayr, & Gail 1993; Gauger, Gail, & Sedlmayr 1990). It is possible to remove these assumptions, or to consider compositions with nonsolar mixes of the metals, within the context of specific models if sufficient information is provided from the model. Some of these effects may require an iteration between the computation of the opacities and the construction of the models. These effects will be pursued in collaboration with other investigators as the opportunity arises.

This work was supported in part by grants from the National Science Foundation (AST-9217946) and the Space Telescope Science Institute (GO-4685). D. R. A. thanks the faculty of the Astronomy Department of Indiana University for their hospitality during his sabbatical leave. We thank H. R. Johnson for many discussions and his constant encouragement of this work. We thank F. Allard, R. A. Bell, A. Borysow, D. Goorvitch, C. A. Iglesias, U. G. Jørgensen, R. L. Kurucz, J. E. Littleton, F. J. Rogers, and M. J. Seaton for sharing their opacity results with us and for many fruitful discussions.

REFERENCES

Alexander, D. R. 1975, ApJS, 29, 363
Alexander, D. R., Augason, G. C., & Johnson, H. R. 1989, ApJ, 345, 1014
Alexander, D. R., & Ferguson, J. W. 1994, in Molecules in the Stellar Environment, ed. U. G. Jørgensen (Berlin: Springer), 149
Alexander, D. R., Johnson, H. R., & Rypma, R. L. 1983, ApJ, 272, 773 (AJR)
Allard, F., Hauschildt, P. H., Miller, S., & Tennyson, J. 1994, ApJ, 426, L39
Anders, E., & Grevesse, N. 1989, Geochim. Cosmochim. Acta, 53, 197
Auman, J. R. 1967, ApJS, 14, 171
Avrett, E. H. 1987, private communication (referenced in Johnson et al. 1988)
Bell, K. L., & Berrington, K. A. 1987, J Phys. B, 20, 801
Bell, R. A. 1979, private communication (referenced in Brown et al. 1989)
———. 1994, Newsl. Analysis Astron. Spectra, 20, 17
Bohren, C. F., & Huffman, D. R. 1983, Absorption and Scattering of Light by Small Particles (New York: Wiley)
Borysow, A., & Frommhold, L. 1989, ApJ, 341, 549
———. 1990, ApJ, 348, L41
Borysow, A., Frommhold, L., & Moraldi, M. 1989, ApJ, 336, 495
Brown, J. A., Johnson, H. R., Alexander, D. R., Cutright, L., & Sharp, C. M. 1989, ApJS, 71, 623
Cameron, A. G. W., & Pines, M. R. 1973, Icarus, 18, 377
Chandra, S., Gaur, V. P., & Pande, M. C. 1991, J. Quant. Spect. Rad. Trans., 45, 57
Cox, A. N., & Stewart, J. N. 1965, ApJS, 19, 243
Cox, A. N., & Tabor, J. E. 1976, ApJS, 31, 271
Dalgarno, A., & Lane, N. F. 1966, ApJ, 145, 623
Dominik, C., Sedlmayr, E., & Gail, H.-P. 1993, A&A, 277, 578
Gauger, A., Gail, H.-P., & Sedlmayr, E. 1990, A&A, 235, 345
Goorvitch, D., & Chackerian, Jr., C. 1994, ApJS, 91, 483
Grevesse, N. 1991, in Evolution of Stars: The Photospheric Abundance Connection, ed. G. Michaud & A. Tutukov (Dordrecht: Kluwer), 63
Griem, H. R. 1960, ApJ, 132, 883
———. 1967, ApJ, 147, 1092
Grossman, L. 1972, Geochim. Cosmochim. Acta, 36, 597
Gurvich, L. V., & Glushko, V. P. 1982, Termodinamicheskie Svoistva Individual'nikh Veschev, Vol. 4 (Moscow: Soviet Acad. Sci.)
Iglesias, C. A. 1993, private communication
Iglesias, C. A., & Rogers, F. J. 1991, ApJ, 371, 408
Iglesias, C. A., Rogers, F. J., & Wilson, B. G. 1990, ApJ, 397, 717
Irwin, A. W. 1987, A&A, 182, 348
Irwin, A. W. 1988, A&AS, 74, 145
John, T. L. 1988, A&A, 193, 189
Johnson, H. R. 1994, in Molecules in the Stellar Environment, ed. U. G. Jørgensen (Berlin: Springer-Verlag), 234
Johnson, H. R., Luttermoser, D. G., & Faulkner, D. R. 1988, ApJ, 332, 421
Johnson, H. R., & Sauval, A. J. 1982, A&AS, 49, 77
Johnson, P. B., & Christy, R. W. 1974, Phys. Rev., 9B, 5056
Jørgensen, U. G. 1990, private communication
———. 1993, private communication
———. 1994a, A&A, 284, 179
———. 1994b, in Molecules in the Stellar Environment, ed. U. G. Jørgensen (Berlin: Springer-Verlag), 29
Jørgensen, U. G., Almlöf, J., Gustafsson, B., Larsson, M., & Siegbahn, P. 1985, J. Chem. Phys., 83, 3034
Jørgensen, U. G., & Jensen, P. 1993, J. Molec. Spectrosc., 161, 219
Jørgensen, U. G., Jensen, P., & Sørensen, G. O. 1994, in Poster Proc. of IAU Colloq. 146, ed. P. Thejll & U. G. Jørgensen (Copenhagen: Neils Bohr Institute), 51
Jørgensen, U. G., & Larsson, M. 1990, A&A, 238, 424
Kim, S.-H., Martin, P. G., & Hendry, P. D. 1994, ApJ, 422, 164
Kurucz, R. L. 1970, Smithsonian Astrophys. Obs. Spec. Rep. 309 (K70)
———. 1991, Stellar Atmospheres: Beyond Classical Models, ed. L. Crivellari, I. Hubeny, & D. G. Hummer (Dordrecht: Reidel), 441
———. 1992, Rev. Mexicana Astron. Af., 23, 181
Kurucz, R. L., & Peytreman, E. 1975, Smithsonian Astrophys. Obs. Spec. Rep. 362
Lenzuni, P, Chernoff, D. F., & Salpeter, E. E. 1991, ApJS, 76, 759
Lenzuni, P., & Saumon, D. 1992, Rev. Mexicana Astron. Af., 23, 223
Littleton, J. E. 1987, private communication
Littleton, J. E., & Davis, S. P. 1985, ApJ, 296, 152
Littleton, J. E., Davis, S. P., & Song, M. 1993, ApJ, 404, 412
Lopez Piñeiro, A., Tipping, R. H., & Chackerian, Jr., C. 1987a, J. Molec. Spectrosc., 125, 91
———. 1987b, J. Molec. Spectrosc, 125, 184
Mathis, J. S., Rumple, W., & Nordsieck, K. H. 1977, ApJ, 217, 425
Ordal, M. A., Bell, R. J., Alexander, Jr., R. W., Newquist, L. A., & Querry, M. R. 1988, Appl. Opt., 27, 1203
Ossenkopf, V., Henning, Th., & Mathis, J. S. 1992, A&A, 261, 567
Pégourié, B. 1988, A&A, 194, 335

© American Astronomical Society • Provided by the NASA Astrophysics Data System

1994ApJ...437..879A

Plez, B. 1992, A&AS, 94, 527
Pollack, J. B., Hollenbach, D., Beckwith, S., Simonelli, D. P., Roush, T., & Fong, W. 1994, ApJ, 421, 615
Pollack, J. B., McKay, C. P., & Christofferson, B. M. 1985, Icarus, 64, 471
Rogers, F. J., & Iglesias, C. A. 1992, ApJS, 79, 507 (OPAL)
Rouleau, F., & Martin, P. G. 1991, ApJ, 377, 526
Sauval, A. J., & Tatum, J. B. 1984, ApJS, 56, 193
Seaton, M. J., Yan, Y., Mihalas, D., & Pradhan, A. K. 1994, MNRAS, 266, 805 (OP)
Sharp, C. M. 1981, Ph.D. thesis, Univ. St. Andrews
———. 1984, A&AS, 55, 33
———. 1989, private communication
———. 1992, A&AS, 94, 1
Sharp, C. M., & Huebner, W. F. 1990, ApJS, 72, 417
Sidhu, K. S., Miller, S., & Tennyson, J. 1992, A&A, 255, 453
Smith, V. V., & Lambert, D. L. 1985, ApJ, 294, 326
———. 1986, ApJ, 311, 843
———. 1990, ApJS, 72, 387
Tipping, R. H. 1987, private communication
Tipping, R. H., & Chackerian, Jr., C. 1981, J. Molec. Spectrosc., 88, 352
Unsöld, A. 1955, Physik der Sternatmospharen (Berlin: Springer-Verlag)
Vernazza, J. E., Avrett, E. H., & Loeser, R. 1980, ApJS, 45, 635
Weiss, A., Keady, J. J., & Magee, Jr., N. H. 1990, Atomic Data Nucl. Data Tables, 45, 209
Wishart, A. W. 1979, MNRAS, 187, 59
Zheng, C., & Borysow, A. 1994, ApJ, submitted

© American Astronomical Society • Provided by the NASA Astrophysics Data System